

The universal function of the diffractive process in color dipole picture

Z. Jalilian* and G. R. Boroun†

Department of Physics, Razi University, Kermanshah, 67149, Iran

(Dated: October 9, 2020)

In this presentation, we obtain the corresponding universal function to the diffractive process and show the cross section exhibits the geometrical scaling. It is observed the diffractive theory according to the color dipole approach at small- x is a convenient framework that reveals the color transparency and the saturation phenomena. Also we calculate the contribution of heavy quark productions in the diffractive cross section for high energy that is determined by the small size dipole configuration. The ratio of the diffractive cross section to the total cross section in the electron-proton collision is the other important quantity that is computed in this work.

1. INTRODUCTION

The color dipole formalism in QCD prediction for high energy deep inelastic scattering at small- x has promoted a lot of phenomenological activity successfully, in recent years. The saturation effect in $x < 0.01$ dominates by the gluon dynamics that describes the details of the electron-proton collision data collected at HERA well [1-4].

Understand the diffractive deep inelastic scattering is a great theoretical feature because 10 to 15 percent of all events observed at HERA are diffractive [5-7]. Many of the experimental data can be explained by perturbative QCD, but an extrapolation to diffractive reactions must carefully be performed because the most of them are sensitive to details of non-perturbative dynamics. The study on the diffraction process comes from pioneering work of Glauber [8] that developed by Good and Walker as a quantum mechanical effect [9].

Indeed, at small- x a diffractive process in DIS, in the electron-proton collision, occurs in the form of $eP \rightarrow eXP$. The dynamics behind this event is simply justified if we review it in the rest frame of the proton. In this case the target proton remains intact, a photon with virtuality Q^2 develops a partonic fluctuation and is forced to a strong interaction with the proton as $\gamma^*p \rightarrow Xp$, so a large rapidity gap (LRG) appears between the scattered proton and particle flow formed from the virtual photon in the final state.

From the perspective of the color dipole approach we can express: when $x \rightarrow 0$, in the rest frame of the target, the virtual photon splits up to a quark-antiquark pair before the scattering tagged with Fock eigenstate $|q\bar{q}\rangle$. This eigenstate is expressed by the quantum mechanical

wave function with probability

$$\begin{aligned} |\Psi_T(z, r)|^2 &= {}_T\langle q\bar{q}|q\bar{q}\rangle_T \\ &= \frac{N_c\alpha_{em}}{2\pi^2} \sum_q e_q^2 [(z^2 + (1-z)^2)\varepsilon^2 K_1^2(\varepsilon r) \\ &\quad + m_q^2 K_0^2(\varepsilon r)], \end{aligned} \quad (1)$$

for the transversely and

$$\begin{aligned} |\Psi_L(z, r)|^2 &= {}_L\langle q\bar{q}|q\bar{q}\rangle_L \\ &= \frac{N_c\alpha_{em}}{2\pi^2} \sum_q e_q^2 4Q^2 z^2 (1-z)^2 K_0^2(\varepsilon r), \end{aligned} \quad (2)$$

for the longitudinally polarized photon.

In above-mentioned equations the fraction of the momentum carrying by quark, z , and the relative transverse separation of the $q\bar{q}$ pair, r , are appropriate freedom degrees. The contribution of each quark flavor is proportional to its electromagnetic charge and inverse mass, $N_c = 3$, $\varepsilon^2 = z(1-z)Q^2 + (m_q)^2$ and the center of mass energy squared of γ^*p is W^2 that $x = \frac{Q^2 + 4m_q^2}{W^2}$. Also for $\varepsilon r < 1$, $K_{1,0}(\varepsilon r)$ is estimated by MacDonald Bessel functions [10].

These equations include Gribov inelastic shadowing corrections to all of multiple interactions what is hardly possible within hadronic presentation [11]. For a dipole-proton interaction we use the dedicated cross section formulated by Bartels, Golec-Bierant and Kowalski as a suitable definition which involves the gluon distribution function [12]

$$\sigma_{q\bar{q}P}(x, r^2) = \sigma_0 \left\{ 1 - \exp\left(-\frac{\pi^2 r^2 \alpha_s(\mu^2) x g(x, \mu^2)}{3\sigma_0}\right) \right\}, \quad (3)$$

with $\mu^2 = \mu_0^2 + \frac{C}{r^2}$ that parameters C and μ_0^2 from fit to DIS data are determined. The dipole-hadron cross

*Electronic address: zeinab.jalilian.kr@gmail.com

†Electronic address: boroun@razi.ac.ir, grboroun@gmail.com

section $\sigma_{q\bar{q}P}$ contains information about the strong interaction physics and the target. In fact, we note the polarized photon in addition to the transverse and the longitudinal photon quark-antiquark pairs can be split up to a transverse $q\bar{q}g$ dipole dominated in final state due to the gluon production. We know the importance of this contribution that has been studied in references [13,14] for nucleon and nucleus, of course, in a different way than our method. Since the $q\bar{q}g$ dipole is created by assuming a strong ordering in the transverse space r the fraction of the momentum carrying by the gluon comparing with the corresponding value for the quark and antiquark is much smaller and we can ignore it. In the other word the most of the energy is carried by the hadron and the virtual photon has just enough energy to dissociate into a $q\bar{q}$ pair before the scattering. Thus the diffractive deep inelastic scattering cross section is formulated as

$$\int_{-\infty}^0 dt e^{B_D t} \frac{d\sigma_{T,L}^D}{dt} \Big|_{t=0} = \frac{1}{B_D} \frac{d\sigma_{T,L}^D}{dt} \Big|_{t=0}, \quad (4)$$

by considering a factorization dependence on t with the diffractive slope B_D [15]. Where

$$\frac{d\sigma_{T,L}^D}{dt} \Big|_{t=0} = \frac{1}{16\pi} \left(\langle \sigma_{q\bar{q}P}^2(x, r^2) \rangle_{T,L} - \langle \sigma_{q\bar{q}P}(x, r^2) \rangle_{T,L}^2 \right). \quad (5)$$

The definition of the expectation value is

$$\begin{aligned} \langle \sigma_{q\bar{q}P}(x, r^2) \rangle_{T,L} &= {}_{L,T} \langle q\bar{q} | \sigma_{q\bar{q}P}(x, r^2) | q\bar{q} \rangle_{T,L}, \\ &= \sigma_{T,L}^{\gamma^* P}(x, Q^2), \\ &= \int_0^1 dz \int d^2r |\Psi_{T,L}(z, r)|^2 \sigma_{q\bar{q}P}(x, r^2). \end{aligned} \quad (6)$$

Since $\langle \sigma_{q\bar{q}P}(x, r^2) \rangle_{T,L} = O(\alpha_{em})$ we can ignore the second term of Eq. (5) in comparison to the first one and hence we will obtain

$$\begin{aligned} \frac{d\sigma_{T,L}^D}{dt} \Big|_{t=0} &= \frac{1}{16\pi} \left(\langle \sigma_{q\bar{q}P}^2(x, r^2) \rangle_{T,L} \right), \\ &= \frac{1}{16\pi} \int_0^1 dz \int d^2r |\Psi_{T,L}(z, r)|^2 \sigma_{q\bar{q}P}^2(x, r^2). \end{aligned} \quad (7)$$

That's mean the diffractive cross section is a quantum mechanics summation over the effective dipole cross section square, $\sigma_{q\bar{q}P}^2(x, r^2)$, for different Fock states [16]. The content of this paper is the following. In section 2 we calculate the diffractive cross section and the universal function and investigate existence of the geometrical scaling. Since the presence of the heavy pairs in the high energy is important we obtain their contribution in section 3. Also in this section the ratio

of the diffractive cross section to the total cross section is determined by the ratio of the corresponding universal functions. Finally results in section 4 are summarized.

2. THE DIFFRACTIVE UNIVERSAL FUNCTION

Before computing, we introduce the x -dependence saturation radius, $R_0(x)$, related to the saturation scale, Q_s , is a energy-dependent scale and is a critical element in determining the saturation point

$$R_0^2(x) = \frac{1}{Q_0^2} \left(\frac{x}{x_0} \right)^\lambda = \frac{1}{Q_s^2}. \quad (8)$$

Positive and constant variables Q_0 , x_0 and λ have been obtained by fitting done with H1 and ZEUS data by Golec-Bierant and Wüthoff [17].

According to Eq. (3) the selection of the gluon distribution is important. For small- r , $r < R_0(x)$, the gluon distribution is modelled as

$$xg(x, \mu^2) = \frac{3\sigma_0}{4\pi^2 \alpha_s R_0^2(x)}, \quad (9)$$

where μ^2 behaves as $\frac{C}{r^2}$. Then for small- r

$$\sigma_{q\bar{q}P}(x, r^2) = \sigma_0 \frac{r^2}{R_0^2(x)}. \quad (10)$$

For larg- r the scale μ^2 is closed to μ_0^2 and according to the original saturation model the saturation value of the dipole cross section is $\sigma_{q\bar{q}P}(x, r^2) \approx \sigma_0$ [18, 19]. We can summarize the contents as

$$\sigma_{q\bar{q}P}(x, r^2) = \begin{cases} \sigma_0, & r > R_0 \\ \sigma_0 \frac{r^2}{R_0^2}, & r < R_0 \end{cases} \quad (11)$$

that we have obtained the saturation cross section, σ_0 , in agreement with data reported by H1 and ZEUS, for more details see Ref [20].

Now we are ready to determine the diffractive cross section. Since the $q\bar{q}$ pairs with the size $r^2 \sim \frac{1}{\varepsilon^2} \cong \frac{1}{Q^2 z(1-z)}$ make the dominant contribution we need to solve the integral of Eq. (7) for $\varepsilon r < 1$ with $0 \leq z \leq 1$.

There are two limit states which are interesting to investigate: one of them is the symmetric pairs with $r \leq 1/Q$ in this case the quark and antiquark carry the equal contribution of the photon transverse momentum. The size of this type of the color dipole is small in comparison to the saturation radius, $r < R_0$, by substituting relations (1), (2) and (11) in Eq.(7) we can obtain the summation over the transverse and longitudinal

contributions

$$\begin{aligned}
\frac{d\sigma_{tot}^D}{dt}|_{t=0} &= \frac{d\sigma_T^D}{dt}|_{t=0} + \frac{d\sigma_L^D}{dt}|_{t=0}, \\
&= \frac{3\alpha_{em}}{32\pi^3} \sigma_0^2 \sum_q e_q^2 \left\{ \int_0^1 dz (z^2 + (1-z)^2) \right. \\
&\quad \times \int_0^{Q^2} d^2 r \varepsilon^2 \left(\frac{1}{\varepsilon^2 r^2} \right) \left(\frac{r^2}{R_0^2(x)} \right)^2 \\
&\quad + \int_0^1 dz \int_0^{Q^2} d^2 r m_q^2 \left(\frac{r^2}{R_0^2(x)} \right)^2 \\
&\quad + \int_0^1 dz 4Q^2 z^2 (1-z)^2 \\
&\quad \times \left. \int_0^{Q^2} d^2 r \left(\frac{r^2}{R_0^2(x)} \right)^2 \right\}, \\
&= \frac{3\alpha_{em}}{32\pi^2} \sigma_0^2 \frac{1}{3Q^4 R_0^4(x)} \sum_q e_q^2 \left\{ \frac{17}{15} + \frac{m_q^2}{Q^2} \right\}. \tag{12}
\end{aligned}$$

We see the diffractive cross section is as small as $\frac{1}{Q^4}$ therefore the main contribution comes from rare fluctuations of photon that corresponds to the color transparency configuration which happens rarely. The idea of the geometrical scaling has been based on writing the total cross section as a function of the dimensionless variable τ as [15]

$$\sigma_{T,L}^{\gamma^*P}(x, Q^2) = \sigma_0 f(\tau). \tag{13}$$

In this work, we select the scaling variable as $\tau = R_0^2(x)Q^2$ and generalize this idea to the diffractive cross section and write in a similar way

$$\frac{d\sigma_{tot}^D}{dt}|_{t=0} = \sigma_0^2 g(\tau), \tag{14}$$

Then Eq. (12) is rewritten as

$$\frac{d\sigma_{tot}^D}{dt}|_{t=0} = \frac{3\alpha_{em}}{32\pi^2} \sigma_0^2 \frac{1}{3\tau^2} \sum_q e_q^2 \left\{ \frac{17}{15} + \frac{m_q^2}{Q^2} \right\}. \tag{15}$$

that

$$g(\tau) = \frac{3\alpha_{em}}{32\pi^2} \frac{1}{\tau^2} \sum_q e_q^2 \left\{ \frac{17}{45} + \frac{m_q^2}{3Q^2} \right\}. \tag{16}$$

To continue we obtain the total diffractive cross section where the dipole size is larger than the saturation radius

$$\begin{aligned}
\frac{d\sigma_{tot}^D}{dt}|_{t=0} &= \frac{d\sigma_T^D}{dt}|_{t=0} + \frac{d\sigma_L^D}{dt}|_{t=0}, \\
&= \frac{3\alpha_{em}}{32\pi^3} \sigma_0^2 \sum_q e_q^2 \left\{ \int_0^1 dz (z^2 + (1-z)^2) \right. \\
&\quad \times \int_0^{R_0^2} d^2 r \varepsilon^2 \left(\frac{1}{\varepsilon^2 r^2} \right) \left(\frac{r^2}{R_0^2(x)} \right)^2 \\
&\quad + \int_0^1 dz \int_0^{R_0^2} d^2 r m_q^2 \left(\frac{r^2}{R_0^2(x)} \right)^2 \\
&\quad + \int_0^1 dz (z^2 + (1-z)^2) \int_{R_0^2}^{Q^2} d^2 r \varepsilon^2 \left(\frac{1}{\varepsilon^2 r^2} \right) \\
&\quad + \int_0^1 dz \int_{R_0^2}^{Q^2} d^2 r m_q^2 \\
&\quad + \int_0^1 dz 4Q^2 z^2 (1-z)^2 \int_0^{R_0^2} d^2 r \left(\frac{r^2}{R_0^2(x)} \right)^2 \\
&\quad + \left. \int_0^1 dz 4Q^2 z^2 (1-z)^2 \int_{R_0^2}^{Q^2} d^2 r \right\}, \\
&= \frac{3\alpha_{em}}{32\pi^2} \sigma_0^2 \sum_q e_q^2 \left\{ \frac{1}{3} \left(\frac{7}{5} - \log(R_0^2 Q^2) \right)^2 \right. \\
&\quad \left. - \frac{4R_0^2 Q^2}{15} + \frac{m_q^2}{Q^2} \left(1 - \frac{2R_0^2 Q^2}{3} \right) \right\}. \tag{17}
\end{aligned}$$

$g(\tau)$ in this case by ignoring the logarithmic sentence is expressed by

$$g(\tau) = \frac{3\alpha_{em}}{32\pi^2} \sum_q e_q^2 \left\{ \frac{7}{15} - \frac{4\tau}{45} + \frac{m_q^2}{Q^2} \left(1 - \frac{2\tau}{3} \right) \right\}. \tag{18}$$

This function when $\tau \rightarrow 0$ becomes

$$g(\tau) = \frac{3\alpha_{em}}{32\pi^2} \sum_q e_q^2 \left\{ \frac{7}{15} + \frac{m_q^2}{Q^2} \right\}. \tag{19}$$

therefore

$$g(\tau) \cong O(\alpha_{em}). \tag{20}$$

We have plotted the ratio $\frac{g(\tau)}{\alpha_{em}}$ for Eqs. (16) and (18) in terms of τ variable in Fig. 1 in different x values for light flavors with $m_q = 140$ MeV. According to these diagrams $\tau = 1$ divides the plane to the saturation and scaling areas and all of them are independent of x . Also we see the slope each diagram in the scaling region is steeper

in comparison to the corresponding universal function to the total cross section, for more information see Ref. [20]. We can briefly express if r changes from $r > R_0$ to $r < R_0$ the unitarity effect in $0 < \tau < 1$ region links to a weak interaction in $\tau \geq 1$, on the other hand the universal function in Fig. 1 behaves as the following

$$\frac{g(\tau)}{\alpha_{em}} \sim 1 \longrightarrow \frac{g(\tau)}{\alpha_{em}} \sim \frac{1}{\tau^2}. \quad (21)$$

The other limit state occurs when one of the components of the pair carries a large part of the transverse momentum. The color dipole created in this case is called the asymmetric pair. We note the condition $\varepsilon r < 1$ in Eq. (7) is fulfilled only if $z < \frac{1}{r^2 Q^2}$ also there must be a cut-off such as $\mu^2 \simeq 4m_q^2$ on the energy. Where the asymmetric dipole size is smaller than the saturation radius we will have

$$\begin{aligned} \frac{d\sigma_{tot}^D}{dt}|_{t=0} &= \frac{d\sigma_T^D}{dt}|_{t=0} + \frac{d\sigma_L^D}{dt}|_{t=0}, \\ &= \frac{3\alpha_{em}}{32\pi^3} \sigma_0^2 \sum_q e_q^2 \left\{ \int_{1/\mu^2}^{1/Q^2} d^2 r \varepsilon^2 \left(\frac{1}{\varepsilon^2 r^2} \right) \right. \\ &\quad \times \int_0^1 r^2 Q^2 dz (z^2 + (1-z)^2) \left(\frac{r^2}{R_0^2(x)} \right)^2 \\ &\quad + \int_{1/\mu^2}^{1/Q^2} d^2 r \int_0^1 r^2 Q^2 dz 4Q^2 z^2 (1-z)^2 \left(\frac{r^2}{R_0^2(x)} \right)^2 \Big\}, \\ &\quad + \int_{1/\mu^2}^{1/Q^2} d^2 r m_q^2 \int_0^1 r^2 Q^2 dz \left(\frac{r^2}{R_0^2(x)} \right)^2 \\ &= \frac{3\alpha_{em}}{32\pi^2} \sigma_0^2 \frac{\sum_q e_q^2}{Q^4 R_0^4(x)} \left\{ \frac{29}{15} + \frac{1}{3} \log \left(\frac{\mu^2}{Q^2} \right) \right. \\ &\quad \left. - \frac{4\mu^2}{3Q^2} + \frac{2\mu^4}{5Q^4} + \frac{m_q^2}{2Q^2} \left(1 - \frac{Q^4}{\mu^4} \right) \right\}. \end{aligned}$$

According to the high power of the virtuality, this function falls much faster than the corresponding case in small pairs and the interaction is almost unexpected. The universal function in this case is given by

$$\begin{aligned} g(\tau) &= \frac{3\alpha_{em}}{32\pi^2} \frac{1}{\tau^2} \sum_q e_q^2 \left\{ \frac{29}{15} + \frac{1}{3} \log \left(\frac{\mu^2}{Q^2} \right) \right. \\ &\quad \left. - \frac{4\mu^2}{3Q^2} + \frac{2\mu^4}{5Q^4} + \frac{m_q^2}{2Q^2} \left(1 - \frac{Q^4}{\mu^4} \right) \right\}. \end{aligned} \quad (23)$$

Finally we investigate the asymmetric pair where its size is large in comparison to the saturation radius

$$\begin{aligned} \frac{d\sigma_{tot}^D}{dt}|_{t=0} &= \frac{d\sigma_T^D}{dt}|_{t=0} + \frac{d\sigma_L^D}{dt}|_{t=0}, \\ &= \frac{3\alpha_{em}}{32\pi^3} \sigma_0^2 \sum_q e_q^2 \left\{ \int_{1/\mu^2}^{R_0^2} d^2 r \varepsilon^2 \left(\frac{1}{\varepsilon^2 r^2} \right) \right. \\ &\quad \times \int_0^1 r^2 Q^2 dz (z^2 + (1-z)^2) \left(\frac{r^2}{R_0^2(x)} \right)^2 \\ &\quad + \int_{1/\mu^2}^{R_0^2} d^2 r m_q^2 \int_0^1 r^2 Q^2 dz \left(\frac{r^2}{R_0^2(x)} \right)^2 \\ &\quad + \int_{R_0^2}^{1/Q^2} d^2 r \varepsilon^2 \left(\frac{1}{\varepsilon^2 r^2} \right) \int_0^1 r^2 Q^2 dz (z^2 + (1-z)^2) \\ &\quad + \int_{R_0^2}^{1/Q^2} d^2 r m_q^2 \int_0^1 r^2 Q^2 dz \\ &\quad + \int_{1/\mu^2}^{R_0^2} d^2 r \int_0^1 r^2 Q^2 dz 4Q^2 z^2 (1-z)^2 \left(\frac{r^2}{R_0^2(x)} \right)^2 \\ &\quad \left. + \int_{R_0^2}^{1/Q^2} d^2 r \int_0^1 r^2 Q^2 dz 4Q^2 z^2 (1-z)^2 \right\}, \\ &= \frac{3\alpha_{em}}{32\pi^2} \sigma_0^2 \sum_q e_q^2 \left\{ \frac{-83}{90} + \frac{2}{R_0^2 Q^2} \right. \\ &\quad + \frac{1}{R_0^4 Q^4} \left(\frac{1}{6} + \frac{1}{3} \log(\mu^2 R_0^2) - \frac{4\mu^2}{3Q^2} + \frac{2\mu^4}{5Q^4} \right) \\ &\quad \left. + \frac{8}{9R_0^6 Q^6} - \frac{1}{5R_0^8 Q^8} + \frac{m_q^2}{2Q^2} \left(1 + \log \left(\frac{1}{Q^2 R_0^2} \right) \right) \right\}, \end{aligned} \quad (24)$$

so the universal function by ignoring the logarithmic sentence is

$$\begin{aligned} (22) \quad g(\tau) &= \frac{3\alpha_{em}}{32\pi^2} \sum_q e_q^2 \left\{ \frac{-83}{90} + \frac{2}{\tau} + \frac{1}{\tau^2} \left(\frac{1}{6} - \frac{4\mu^2}{3Q^2} \right) \right. \\ &\quad \left. + \frac{2\mu^4}{5Q^4} + \frac{8}{9\tau^3} - \frac{1}{5\tau^4} + \frac{m_q^2}{2Q^2} \right\}. \end{aligned} \quad (25)$$

The ratio $\frac{g(\tau)}{\alpha_{em}}$ for the universal functions (23) and (25) in terms of the scaling variable has been plotted in Fig. 2 in the different x values for light quarks. According to these diagrams we can result the diffractive contribution of asymmetric pairs is dominated in the saturation limit so for $0 < \tau < 1$ the system connected to a heavily absorbed diffractive event.

3. THE CONTRIBUTION OF HEAVY QUARKS IN THE DIFFRACTIVE PROCESS

In high energy the heavy flavors are useful in the agreement with the experimental data. A common way for study on the heavy productions has been based on the ratio method which is associated with the geometrical scaling [21]. In pervious section we obtained the diffractive cross section quantitatively and showed by plotting Figs. 1 and 2 the geometrical scaling is established for light quarks. Now we assume the summation over flavors expands to include the charm quark with $m_c = 1.5$ GeV and plot the corresponding fraction $\frac{g(\tau)}{\alpha_{em}}$ in Fig. 3. According to these diagrams we see there is not the dependence on x and all curves almost fall on one, in the other words the geometrical scaling is confirmed. The main cause of the increase in the value of this function is that the charm quark because of its high mass is saturated at a higher order.

Fig. 4 by considering the bottom quark with $m_b = 4.75$ GeV to active flavors has been plotted that shows these diagrams behave similar to ones in Figs. 1 and 3 so the geometrical scaling is fulfilled.

We note, since the heavy production appears in the feature of a symmetric dipole, universal functions (16) and (18) in plotting diagrams are used.

According to H1 and ZEUS reports the charm component of the structure function includes a significant fraction of the proton structure function [22,23]. We calculate the contribution of this flavor in the diffractive cross section

$$\frac{d\sigma_c^D}{dt}|_{t=0} = \frac{g_c(\tau)}{g(\tau)} = \frac{\delta_{qc}(g(\tau))}{g(\tau)}, \quad (26)$$

the δ_{qc} function chooses charm quark from all active flavors. $c\bar{c}$ pair is dominated in small size dipoles with $r < R_0$ so

$$\frac{d\sigma_c^D}{dt}|_{t=0} = \frac{g_c(\tau)}{g(\tau)} = \frac{e_c^2(\frac{17}{45} + \frac{m_c^2}{3Q^2})}{e_c^2(\frac{17}{45} + \frac{m_c^2}{3Q^2}) + (e_u^2 + e_d^2 + e_s^2)(\frac{17}{45} + \frac{(0.140)^2}{3Q^2})}. \quad (27)$$

The average value of the charm production in the diffractive process by assuming $0.037 \leq r_c \leq 0.13$ fm is about 40 percent according to Fig. 5. This figure shows the corresponding fraction is independent of x and Q^2 and all curves fall on one.

We can calculate this fraction for estimating of the bottom production $b\bar{b}$ as

$$\frac{d\sigma_b^D}{dt}|_{t=0} = \frac{g_b(\tau)}{g(\tau)} = \frac{\delta_{qb}(g(\tau))}{g(\tau)}, \quad (28)$$

δ_{qb} selects the bottom quark from five active flavors. Therefore the possibility for finding the bottom production becomes

$$\frac{d\sigma_b^D}{dt}|_{t=0} = \frac{g_b(\tau)}{g(\tau)} = \frac{e_b^2(\frac{17}{45} + \frac{m_b^2}{3Q^2})}{e_b^2(\frac{17}{45} + \frac{m_b^2}{3Q^2}) + e_c^2(\frac{17}{45} + \frac{m_c^2}{3Q^2}) + \frac{2}{3}(\frac{17}{45} + \frac{(0.140)^2}{3Q^2})}, \quad (29)$$

that is about 10 percent in the range $0.014 \leq r_b \leq 0.043$ fm that is seen from Fig.6. In recent relations the important element is $(\frac{m_q^2}{Q^2})$ that along with e_q^2 includes inherent characterizes of the dipole. Also all of curves in Fig. 6 fall on one that means there is not dependence on x and Q^2 .

To continue we can take a step forward and obtain the ratio of the diffractive cross section to the total cross section [20]. For symmetric dipoles with $r < R_0$ we get

$$R(\tau) = \frac{d\sigma_{tot}^D}{dt}|_{t=0} = \frac{\sigma_0^2 g(\tau)}{\sigma_{tot}^{\gamma^*P}(x, Q^2)} = \frac{\sigma_0}{16\pi\tau} \left(\frac{\sum_q e_q^2(\frac{17}{45} + \frac{m_q^2}{3Q^2})}{\sum_q e_q^2(\frac{11}{15} + \frac{m_q^2}{2Q^2})} \right), \quad (30)$$

and where $r > R_0$ we will have

$$R(\tau) = \frac{d\sigma_{tot}^D}{dt}|_{t=0} = \frac{\sigma_0^2 g(\tau)}{\sigma_{tot}^{\gamma^*P}(x, Q^2)} = \frac{\sigma_0}{16\pi} \left(\frac{\sum_q e_q^2(\frac{7}{15} - \frac{4\tau}{45} + \frac{m_q^2}{Q^2}(1 - \frac{2\tau}{3}))}{\sum_q e_q^2(\frac{4}{5} - \frac{4\tau}{60} + \frac{m_q^2}{Q^2}(1 - \frac{\tau}{2}))} \right). \quad (31)$$

These ratios only relate to the size, mass and charge of color dipoles. We have plotted them in Fig. 7 in terms of the scaling variable, τ , for light flavors. In $0 < \tau < 1$ we see a flat function that for $\tau > 1$ reduces proportionally to $\frac{1}{\tau}$ that express in the diffractive event the saturation is dominated and the interaction in the scaling region occurs rarely. It is necessary to mention there is no dependence on x and Q^2 [24-26]. We expect this behavior also remains by adding the contribution of heavy quarks.

Our other suggestion for showing the ratio of the diffractive cross section to the total cross section is independent of x and Q^2 so we plot $\frac{R(\tau)}{\sigma_0}$ in terms of the center of mass energy of γ^*p , W , as [12]. This quantity in Fig. 8 has been plotted for light quarks with $m_q = 140 MeV$ for different x values. We see a flat function for $W > 100 GeV$ that indicates the invariance of this ratio.

4. SUMMARY

The color dipole picture is an effective field theory in describing the small- x limit of QCD without nonlinear sentences in the evolution equation and connects to the unitarity effect due to the gluon recombination. In this analysis we discuss the diffractive deep inelastic scattering by the color dipole picture. We believe our model represents the basic dynamics because it allows us to study a wide range of data in a satisfactory way. We can assume by following Good and Walker method diffractive eigenstates as colorless quark-antiquark pairs which remain unchanged during the scattering. The diffractive process is characterized by a final state in which a large rapidity gap is not filled with particles. The LRG in the limit of the unitarity saturation may be terminated by the absorptive correction.

We came to the conclusion that in both the symmetric and asymmetric dipoles the diffraction is sensitive to the saturation effect since the diffractive cross section is proportional to σ_0^2 . Fig. 1 shows there is a smooth transfer from the color transparency to the saturation when the scaling variable is around 1. Also in the enough energy by adding the contribution of heavy flavore this transition in Figs. 3 and 4 is seen and the small- x saturation is proven. According to Fig. 2 we conclude that extrapolation to the diffraction process proves the saturation effect well for large-size dipoles and shows the interaction in the scaling region occurs rarely.

The probability of the charm production in $x < 0.01$ directly originated from virtual photon in the diffractive process is about 40 percent. This impressive contribution

expresses the importance of the charm cross section in colliders in the high energy. The corresponding fraction for the bottom production decreases to 10 percent because of small size and large mass of this flavor. From Figs. 5 and 6 we calculate the geometrical scaling is confirmed in the diffractive process including heavy flavores and both of the obtained magnitudes depends on the mass, size and charge of the involved active quarks.

The ratio of the diffractive cross section to the total cross section painted in Fig. 7 is the other quantity depends on inherent characteristics of dipoles and remains unchanged relative to x variable. Fig. 8 is another confirmation to show this ratio is invariance.

The significant conclusion of this work is that the diffractive event in the color dipole model probes QCD in a different way, for instance, the unitarity is an important ingredient associated with the saturation effect that leads to a good description of data.

In conclusion, the idea of the geometrical scaling for the diffractive cross section is in place. The universal functions obtained are not bounded functions and only depends on the inherent properties of dipoles.

REFERENCES

- 1.C. Ewerz and O. Nachtmann, *Annals Phys.* **322**, 1635 (2007) [arXiv:hep-ph/0404254].
- 2.C. Ewerz and O. Nachtmann, *Annals Phys.* **322**, 1670 (2007) [arXiv:hep-ph/0604087].
- 3.H. Kowalski and A. Luszczak, *Phys. Rev.* **D89**, 074051 (2014).
- 4.A. Luszczak and H. Kowalski, *Phys. Rev.* **D953**, 014030 (2017).
- 5.K. Golec-Bierant, *Acta Phys. Polon.* **B53** (2004)[arXiv:hep-ph/0311278v2].
- 6.C. Marquet and L. Schoeffel, *Phys. Lett.* **B639** (2008) [arXiv:hep-ph/0606079].
- 7.Stanley J. Brodsky, Ivan Schmidt and Jian Yang, *Phys. Rev.* **D10**, 116003 (2004) [arXiv:hep-ph/0409279].
- 8.R.J. Glauber, *Phys. Rev.* **100**, 242 (1955).
- 9.M.L. Good and W.D. Walker, *Phys. Rev.* **120**, 1857 (1960).
- 10.V.P. Goncalves and M.V.T. Machado, *Phys.Rev.Lett.* **91**, 202002 (2003) [arXiv:hep-ph/0307090].
- 11.B. Z. Kopeliovich, L. I. Lapidus and A. B. Zamolodchikov, *JETP Lett.* **33**, 595 (1981).
- 12.J. Bartels, K. Golec-Bierant and H. Kowalski, *Phys. Rev.* **D66** (2002).
- 13.C. Marquet, *Phys.Rev.* **D76**, 094017 (2007).
- 14.H. Kowalski, T. Lappi, C. Marquet and R. Venugopalan, *Phys. Rev.* **C78**, 045201 (2008).
- 15.K. Golec-Biernat and M. Wüsthoff, *Phys. Rev.* **D60**, 114023 (1999) [arXiv:hep-ph/9903358].
- 16.M.S. Kugeratski, V.P. Goncalves and F.S. Navarra, *Eur. Phys. J.* **C46** (2006) [arXiv:hep-ph/0511224].
17. S. Aid, et. al. [H1 Collaboration], *Nucl. Phys.* **B470**, (1996); M. Derrick, et. al. [ZEUS Collaboration], *Z. Phys.* **C72**, 399 (1996).
- 18.K. Golec-Biernat and M. Wüsthoff, *Phys. Rev.* **D59**, 014017 (1999).
- 19.K. Golec-Biernat and M. Wüsthoff, *Eur. Phys. J.* **C20**, 313 (2001).
- 20.Z. Jalilian and G.R. Boroun, *Phys. Lett.* **B773**, p.455-461 (2017).
- 21.T. Steble, *Phys. Rev.* **D88**, 014026 (2013).
- 22.V.P. Goncalves, B. Kopeliovich, J. Nemchik, R. Pasechnik and I. Potashnikova, *Phys. Rev.* **D96**, 014010 (2017).
- 23.K. Werner, B. Goiot, lu. Karpenko, T. Pierog and G. Sophys, Conference: C15-11-23, p.66-70, (2016) [arXiv:hep-ph/1602.03414v1]
- 24.K. Golec-Biernat and M. Wüsthoff, *Phys. Rev.* **D59**, 014017 (1998).
- 25.C. Adloff et. al. [H1 Collaboration], *Z. Phys.* **C76**, 6130 (1997).
- 26.J. Braitwey, et. al. [ZEUS Collaboration], *Eur. Phys. J.* **C1**, 810 (1998).

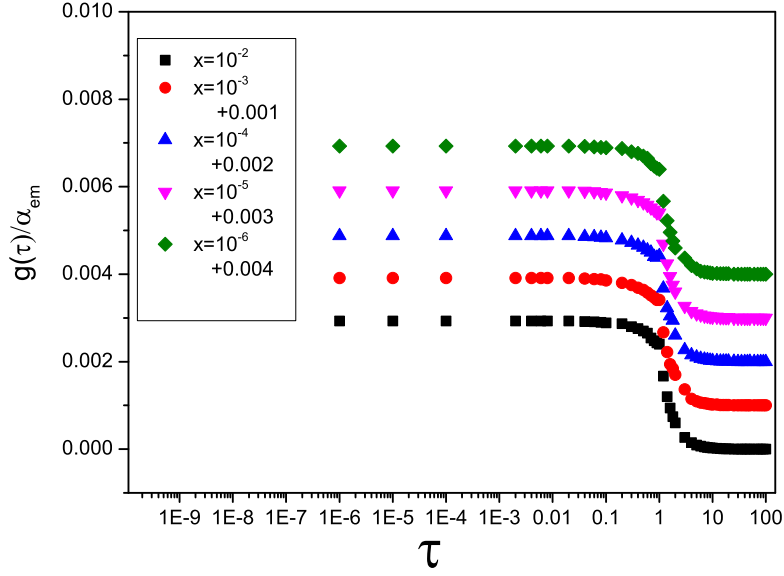


FIG. 1: The ratio $\frac{g(\tau)}{\alpha_{em}}$ for symmetric pairs in the different x values belong to the range $10^{-6} - 10^{-2}$ to τ variable for light flavors.

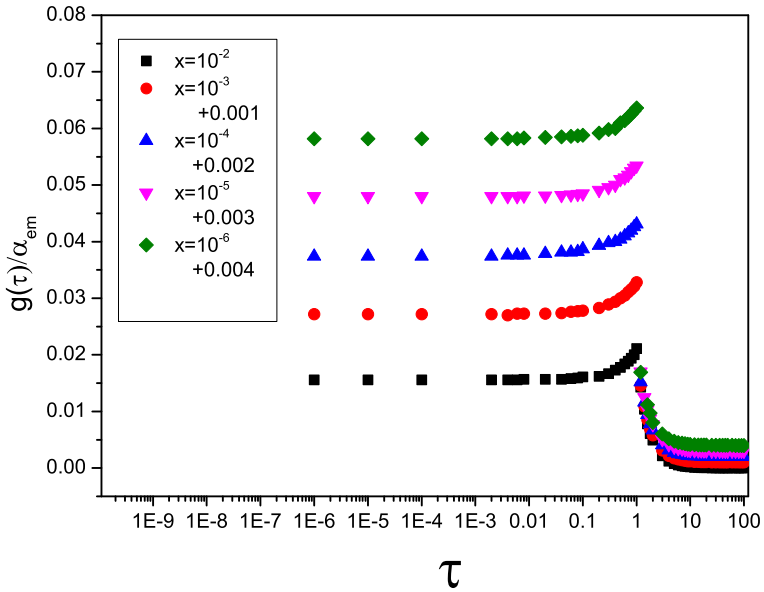


FIG. 2: The ratio $\frac{g(\tau)}{\alpha_{em}}$ for asymmetric pairs in the different x values belong to the range $10^{-6} - 10^{-2}$ to τ variable for light flavors.

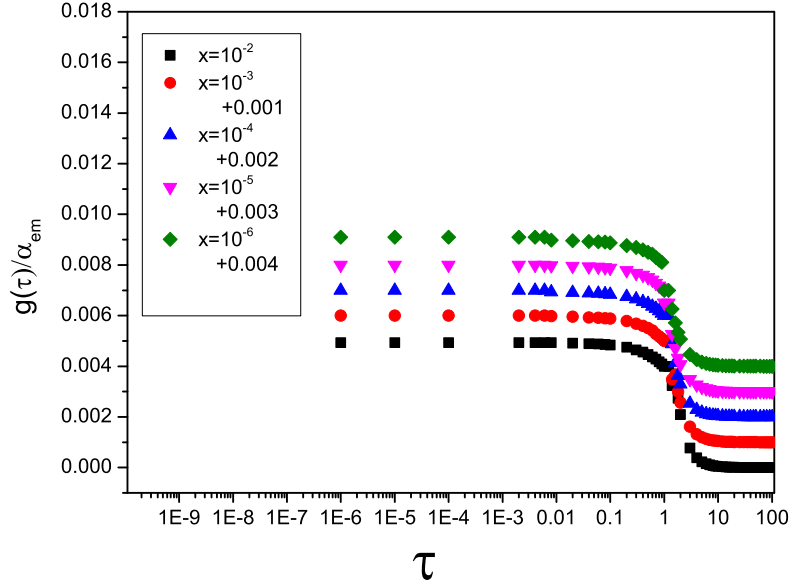


FIG. 3: The ratio $\frac{g(\tau)}{\alpha_{em}}$ by considering light and charm flavors of symmetric dipoles in the different x values belong to the range $10^{-6} - 10^{-2}$ to τ variable.

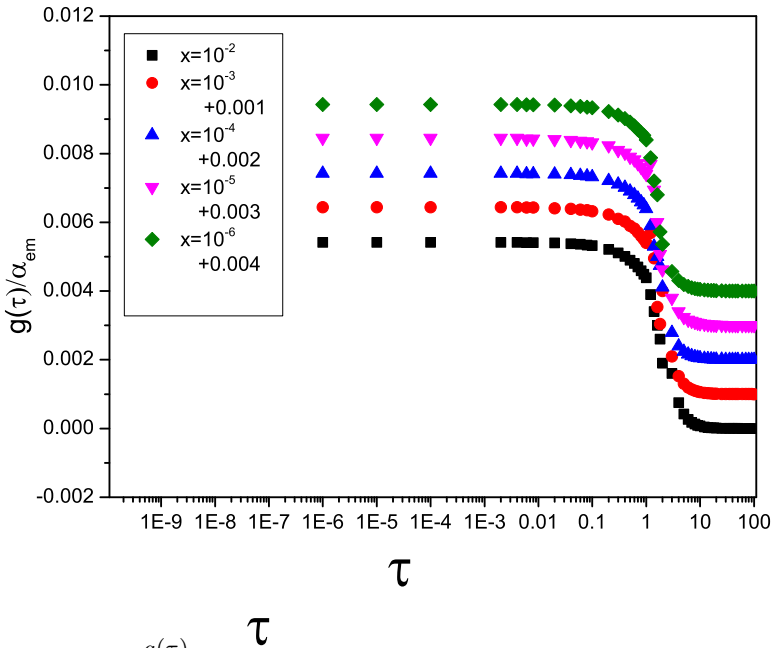


FIG. 4: The ratio $\frac{g(\tau)}{\alpha_{em}}$ by considering light, charm and bottom flavors of symmetric dipoles in the different x values belong to the range $10^{-6} - 10^{-2}$ to τ variable.

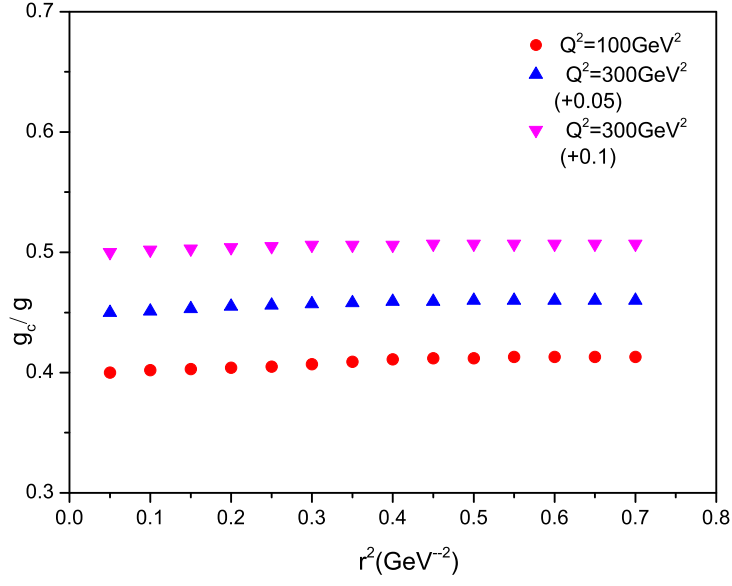


FIG. 5: The contribution of the charm quark in the diffractive cross section for $Q^2 = 100, 200$ and 300 GeV 2 .

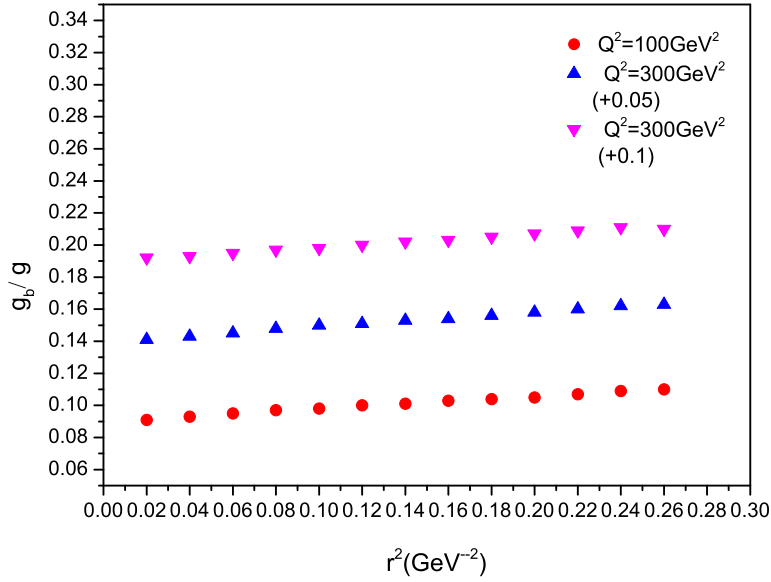


FIG. 6: The contribution of the bottom quark in the diffractive cross section for $Q^2 = 100, 200$ and 300 GeV 2 .

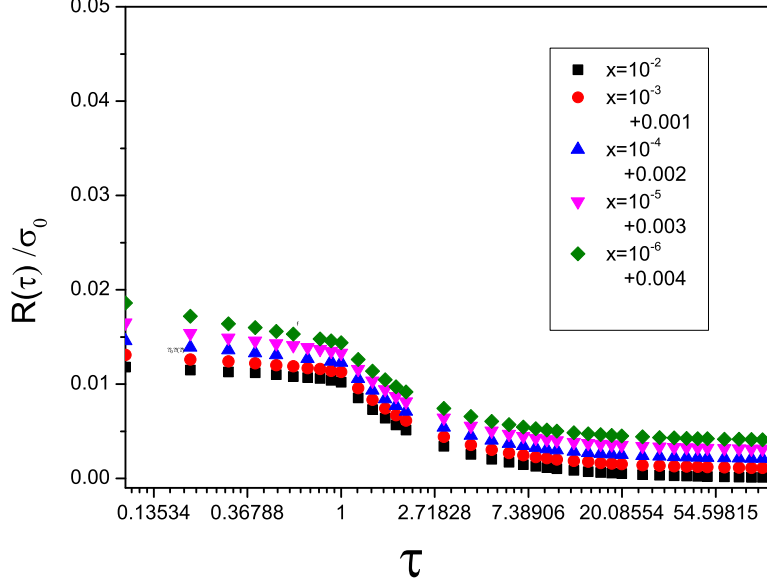


FIG. 7: The ratio $\frac{1}{\sigma_0} \frac{d\sigma_{tot}^D}{dt}|_{t=0} = \frac{R(\tau)}{\sigma_0}$ in the different x values belong to the range $10^{-6} - 10^{-2}$ to τ variable for light flavors.

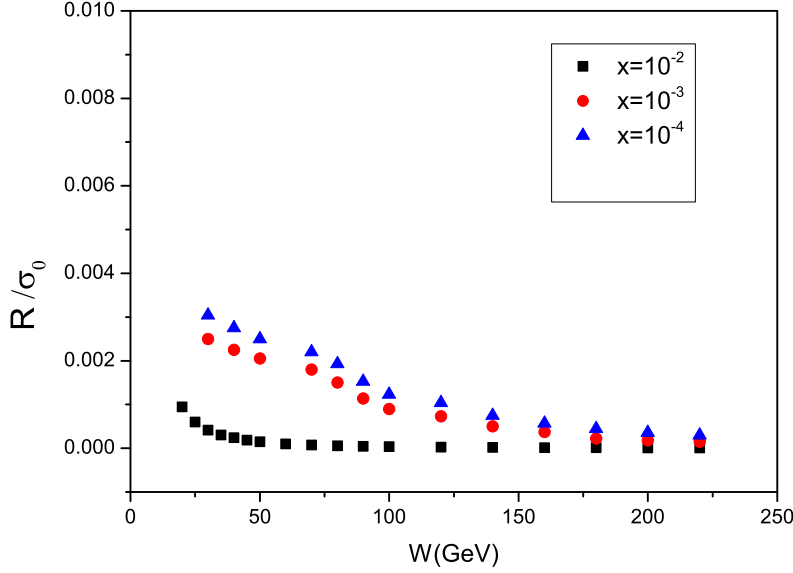


FIG. 8: The ratio $\frac{1}{\sigma_0} \frac{d\sigma_{tot}^D}{dt}|_{t=0} = \frac{R}{\sigma_0}$ in the different x values to the center of mass energy of γ^*p for light flavors.